Proceedings of IMECE2008
2008 ASME International Mechanical Engineering Congress and Exposition
October 31- November 6, 2008, Boston, MA, USA

IMECE2008-66368

BIO-HEAT TRANSFER IN A MODEL SKIN SUBJECT TO A TRAIN OF SHORT PULSE IRRADIATION

Jian Jiao
Department of Mechanical and Aerospace Engineering, Rutgers University
Piscataway, NJ 08854, USA

Zhixiong Guo
Department of Mechanical and Aerospace Engineering, Rutgers University
Piscataway, NJ 08854, USA

ABSTRACT
Thermal analysis of biological tissues subject to a train of ultrashort pulse irradiations was made of developing a combined time-dependent radiation and conduction bio-heat transfer model. A model skin tissue stratified as three layers with different optical, thermal and physiological properties was considered. Temperature response of the skin tissue exposed to a single ultrashort pulse irradiation was firstly analyzed by the finite volume method in combination with the transient discrete ordinates method. This temperature rise was found to reach pseudo steady state within an extremely short time period in which thermal diffusion is negligible. Since the tissue properties were assumed to be constant during a train of pulse irradiation, this temperature rise subject to a single pulse can be employed for repeated pulses. In the same time, Pennes' equation was employed to study the bio-heat transfer in the meso-time scale. The effects of pulse strengths and repetition rate on the temperature response in the multi-layer skin tissue were investigated.

1. INTRODUCTION
Recently short pulsed lasers are considered in a variety of biomedical applications with increasing interests. Comparing with traditional continuous wave lasers, pulsed lasers have additional ability to control the size and depth of a heating zone as well as induce high heating or cooling rates because of higher peak power and shorter interaction time duration.

Short pulsed irradiation is accompanied with the use of ultrafast lasers with pulse width in the range from picoseconds down to femtoseconds. Ultrafast lasers can be used in a wide spectrum of emerging biomedical technologies such as laser surgery treatment[1-4], optical imaging and diagnostics [5-7], etc. Fundamentals to these applications are knowledge of multiple time scale heat transfer processes in biological tissues which include ultrafast laser radiation transport in the nano time scale and transient bio-heat transfer in the meso-time scale.

The concept of ultrafast radiation heat transfer associated with radiation propagation of light was introduced to differentiate the traditional time-dependent radiation heat transfer in which the boundary condition is time-varying but the governing equation of radiative heat transfer is still steady state. Many studies in the literature [8-12] have established the applicability and techniques for solving ultrafast radiation heat transfer problems. A recent work [13] of one of the authors has studied the thermal response of a homogeneous turbid tissue to short pulse irradiation, in which a pulse train within 1ms was considered. Within 1 ms thermal diffusion was neglected and temperature rise in the tissue was calculated. After 1 ms, the whole irradiation was turned off, and conductive heat transfer with thermal wave model was employed to investigate the temperature decay in the tissue. However, there are many cases that require a longer exposure time of irradiation. For example, it may require 1s irradiation exposure to kill completely cancerous cells. And within 1s, thermal diffusion is certainly not negligible.

The presence of vessels is one of the most important points on perfused tissue heat transfer. The Pennes model for describing heat transfer in a perfused tissue has become well known as the bio-heat transfer equation. It assumes that the thermal contribution of blood be modeled as if it entered an imaginary pool at equilibrium with the surrounding tissue. A recent review compared several bio-heat transfer models and concluded that the Pennes model is still the most practical for fast prediction of transient temperature profiles such as those expected in certain hyperthermia conditions [14].

In this article, the combined radiation and Penne's heat transfer model is developed for bio-heat transfer in a skin tissue subject to a pulse train irradiation. An axisymmetric two-dimensional model is considered for the three-layer skin tissue

cylinder. The ultrafast radiative heat transfer model was employed for tissue radiation absorption and scattering subject to a single pulse irradiation. The local temperature rise within a short time without thermal diffusion is obtained using the finite volume method. Between two successive pulses, the temperature field in the tissue is predicted by adopting the Pennes bio-heat transfer model. With the onset of a new pulse, the temperature rise predicted by the single pulse irradiation model is then added to the temperature field and the bio-heat transfer calculation continues. Such a procedure is repeated for all incident pulses. In this manuscript, the effects of pulse train frequency, pulse strengths, metabolic generation rate, and blood perfusion rate are also investigated.

2. NOMENCLATURE

Symbols

a	Radius
c	speed of light
C	specific heat capacity
h	convective heat transfer coefficient
I	radiative intensity
k	Conductivity
L	Depth
M	number of angular discretization
n	refractive index
r	radial direction
R	Reflectance
q	heat flux
S	source term
t	Time
t_p	pulse width
V	Volume
w	angular weight
z	axial direction
θ	azimuthal angle
μ,η,ξ	direction cosine
ρ	Reflectivity
σ_a	absorption coefficient
σ_e	extinction coefficient
σ_s	reduced scattering coefficient
ϕ	circumferential angle
ω	scattering albedo

Subscripts

b	blood perfusion
c	Collimated
d	Diffusive
i	Incidence
l	discrete direction index
m	Metabolism
r	Reflectance
s	Specular
w	Wall

3. MATHEMATICAL MODEL

3.1 Governing Equations

A train of collimated laser short pulses are incident upon a skin tissue cylinder as shown in Fig. 1. The temperature response is governed by the following general energy equation:

$$\rho C_p \frac{\partial T(r,z,t)}{\partial t} = -\nabla\cdot[q_{cond}(r,z,t) + q_{rad}(r,z,t)] + (\rho C)_b \omega_b (T_a - T) + q_M \quad (1)$$

where ρ , C_p , k , T denote the density, specific heat, thermal conductivity and temperature of tissue, respectively; C_b is the specific heat of blood; ω_b is the blood perfusion rate; q_m is the metabolic heat generation; and T_a is the supplying arterial blood temperature.

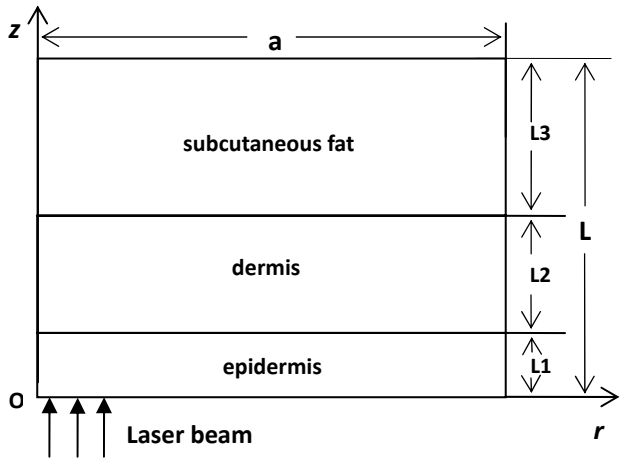

Figure 1 Geometric and coordinate sketches.

The transient radiative transfer equation of intensity I_l in the discrete ordinates direction $\vec{s}_l$ can be formulated as:

$$\frac{1}{c}\frac{\partial I_l}{\partial t} + \frac{\mu_l}{r}\frac{\partial}{\partial r}(rI_l) - \frac{1}{r}\frac{\partial}{\partial \phi}(\eta_l I_l) + \xi_l \frac{\partial I_l}{\partial z} + (\sigma_a + \sigma_s) I_l = (\sigma_a + \sigma_s) S_l \quad l = 1,2,....,M \quad (2)$$

where μ_l , η_l , ξ_l are three directional cosines; σ_a is the absorption coefficient and σ_s is the reduced scattering coefficient; c is the speed of light in the medium, expressed by c/n , n is the refractive index of the tissue; S_l is the radiative source term, which is

$$S_l = (1-\omega) I_b + \frac{\omega}{4\pi} \sum_{i=1}^{M} w_i \Phi_{il} I_l + S_c^l \quad (3)$$

where $\omega = \frac{\sigma_s}{\sigma_s + \sigma_a}$ is the scattering albedo, w_i is the appropriate angular weight in the discrete direction $\vec{s}_i$; Φ_{il} represents scattering phase function

$\Phi(\vec{s_i} \to \vec{s_l})$, S_c^l is the source contribution of collimated irradiation and can be expressed as

$$S_c^l = \frac{1}{4\pi} I_c \Phi(\vec{s_c} \to \vec{s_l}) \tag{4}$$

where the unit vector $\vec{s_c}$ represents the collimated laser incident direction. When the reduced scattering coefficient is used, the scattering function is a unity. In the region where no collimated laser irradiation is passing through, $I_c = S_c^l = 0$.

The incident laser intensity is assumed of temporal and spatial Gaussian profiles and can be expressed as:

$$I_c(r,z,t) = (1-R) I_0 \exp\left\{-4\ln 2 \times [(t - z/c)/t_p - 2]^2\right\} \times \exp(-r^2/v^2) \times \exp(-\sigma_e z) \tag{5}$$

where I_0 is the amplitude of the pulse strength (heat flux), v is the Gaussian variance, t_p is the pulse width, R is the reflectance on the tissue-air inter surface. $\sigma_e = \sigma_s + \sigma_a$ is the reduced extinction coefficient.

In this study, we used a spatially square-variance pulse input, in which the intensity is uniformly spread over the laser beam. Laser parameters used in most cases, if not mentioned, are listed in Table 1.

Table 1 Laser parameters.

Wavelength	Pulse width	Pulse duration
1100nm	10ps	40ps
Spot diameter	Amplitude of pulse	Repetition rate
1mm	1.6E-3 (J/mm^2/ps)	1 kHz

Once the intensity field is obtained, the incident radiation, and the divergence of radiative heat flux can be calculated as:

$$G = \sum_{l=1}^{n} w_l I_l + I_c \tag{6}$$

$$\nabla \cdot q_{rad} = \sigma_a (4\pi I_b - G) \tag{7}$$

During the time between two successive pulses irradiation, the thermal process in the tissue can be divided into two steps:

In the first step, within 400ps, a dimensional analysis reveals that heat diffusion is negligible. A localized temperature rise is induced totally by the single ultrafast pulse irradiation which is described as:

$$\rho C_p \frac{\partial T(r,z,t)}{\partial t} = -\nabla \cdot q_{rad}(r,z,t) \tag{8}$$

In the second step, Penne's equation[14] was used for modeling heat transfer in the skin tissue in the meso-time scale:

$$\rho C_p \frac{\partial T(r,z,t)}{\partial t} = \nabla k \cdot \nabla T + (\rho C)_b \omega_b (T_a - T) + q_m \tag{9}$$

3.2 Boundary conditions

For radiative heat transfer model, we consider two types of radiation boundary conditions for the present problem. The first type is the tissue-air interface. The second type is the tissue-tissue interface. In Figure 1, the laser incident surface (z=0) is considered as the first type of boundary where Fresnel reflection must be considered because of the mismatch of the refractive indices between the tissue and air.

For the normally incident laser radiation, the reflectance on the incident surface is

$$R = \left(\frac{n+1}{n-1}\right)^2, \text{ at z=0} \tag{10}$$

where n is the refractive index of the tissue.

For internal radiation at the tissue-air interface, a critical angle is given by Snell's law:

$$\theta_{cr} = \sin^{-1}(1/n). \tag{11}$$

Total reflection occurs when the incident angle $\theta_i \geq \theta_{cr}$. When $\theta_i < \theta_{cr}$, the reflection on the interface is purely specular and the reflectance is calculated by Fresnel's equation:

$$R_s = \frac{1}{2}\left[\frac{\tan^2(\theta_i - \theta_r)}{\tan^2(\theta_i + \theta_r)} + \frac{\sin^2(\theta_i - \theta_r)}{\sin^2(\theta_i + \theta_r)}\right], \text{ at z=0} \tag{12}$$

θ_r

Surfaces except the laser incident one are all second type interface. Since biological tissues are generally highly scattering, photons reaching the boundary of tissues must have been undergone multiple scattering events and the possibilities of photons passing through the boundary or reflecting back are almost equal. Thus, we specify a diffuse reflectance $R_d = 0.5$ of on such surfaces. The reflecting boundary conditions can be represented by [12, 13]

$$I_w = R_s I_w^{-1} + \frac{R_d}{\pi}\left[I_{cw} + \sum_{\vec{n} \cdot \vec{s_l} < 0} w_l I_{w,l} \left|\vec{n} \cdot \vec{s_l}\right|\right], \tag{13}$$

Along the centerline of the tissue cylinder (r=0), an axisymmetric condition is applied.

For conductive heat transfer model, except for the laser incident surface which is exposed to the ambient air at room temperature of $T_{am} = 25^\circ C$ with convective heat transfer coefficient $h = 15 W/(m^2 \cdot s)$, all other two surfaces of the tissue cylinder are surrounded by tissue remained at $37^\circ C$. Again the centerline of the cylinder is treated as axisymmetric boundary. Thus the initial and boundary conditions for parabolic conduction model are given as follows:

$$T = 37^\circ C, \text{ when } t=0 \tag{14}$$

$$T = 37^\circ C, \text{ at r=a or z=L} \tag{15}$$

$$\frac{\partial T}{\partial r} = 0, \text{ at r=0} \tag{16}$$

$$-k\frac{\partial T}{\partial r} = h(T - T_{am}),\ \text{at z=0} \qquad (17)$$

3.3 Properties of skin tissue

Human skin is organized in distinct layers, which are epidermis, dermis and subcutaneous fat, respectively. Initially, the whole skin tissue is assumed to be at a constant and uniform temperature of $37^{\circ}C$. The physiological, optical and thermal properties of different layers of tissues are listed in Tables 2, 3 and 4, respectively.

Table 2 Physiological parameters for different skin tissue layers[15].

	epidermis	dermis	fat
Perfusion ratio (ml/ml/s)	0	1.63E-3	1 E-3
Metabolic heat generation (W/kg)	1	1	0.32
Thickness (mm)	0.1	0.35	0.65

Table 3 Optical parameters for different tissue layers[16].

	epidermis	dermis	fat
Reduced scattering coefficients (mm^{-1})	2.0	0.9	0.8
Absorption coefficients (mm^{-1})	0.011	0.016	0.1

Table 4 Thermal parameters for different tissue layers in the wavelength 1100 nm [17].

	epidermis	dermis	fat
ρCp ($J/mm^3/K$)	3.77E-3	3.77E-3	1.955E-3
k (W/m/K)	0.21	0.30	0.21

3.4 Numerical Scheme

The TDOM (Transient Discrete Ordinates Method) was employed for the solution of the present radiative heat transfer problem. A quadrature set of M=N(N+2) discrete ordinates is used for the S_N method. In this research, we basically used an S_{10} scheme. Detailed information on numerical scheme and accuracy validation, please refer to literatures[11, 12, 18]. The transient conductive heat transfer equations are solved numerically by using an Alternating Direction Implicit (ADI) scheme [19]

For both the radiation and conduction simulations, the same grid system is adopted to avoid interpolation. The stagger grid size (r, z) was 110×110 for a typical skin tissue cylinder with $a = 5\text{mm}, L = 1.1\text{mm}$. The time step of this typical cylinder was $\Delta t = 0.2\text{ps}$ for radiation simulation and $\Delta t = 0.25\text{ms}$ for conduction simulations, respectively. The heat conduction calculation of the skin tissue subject the pulse train is continuous. While the calculation time of radiation heat transfer is extended to 400ps and only one calculation is needed because the temperature response caused by each short pulse irradiation can be treated as a pure temperature rise in the onset of a new pulse.

Reducing the grid size and time step, which correspondingly increases the number of nodes, checks the stability. Results are found to be convergent.

3.5 Assumptions

In the present model, following assumptions are made:

1. In the time scale within $40t_p$, thermal propagation and diffusion are negligible. The localized temperature response is caused by the pulse irradiation.
2. Tissue radiation emission is neglected comparing with the much stronger incident laser intensity.
3. Tissue optical and thermal properties are thermally stable during the heat transfer process.
4. Suppose no ablation in the whole process.

4. RESULTS AND DISCUSSION

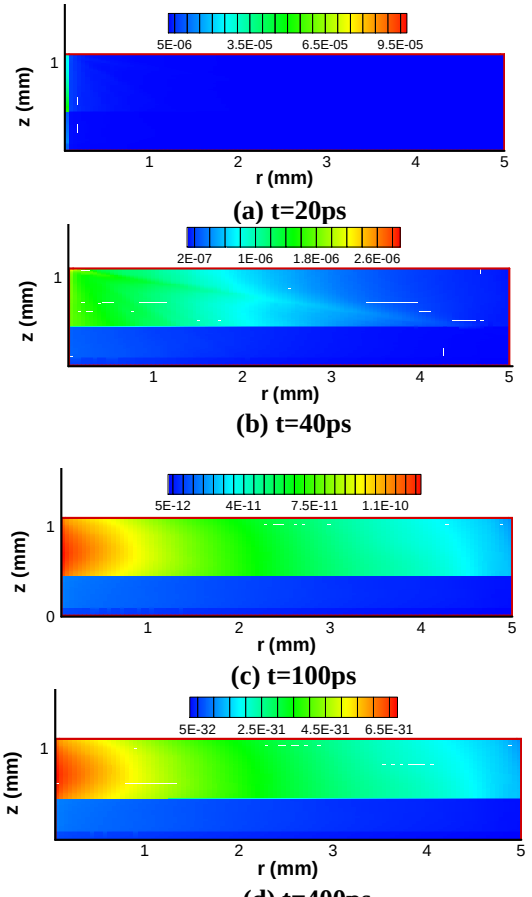

Figure 2 Contours of the divergence of radiative heat flux in the skin tissue subject to one pulse irradiation at selected time instants.

For the ultrafast radiation heat transfer modeling, we consider a pulse width of 10ps. The time step is 0.2ps and calculation time is extended to 400ps. Fig.2 shows the contours of the divergence of radiative heat flux in the multi-layer tissue subject to a pulse at four different time instants. It is noticed that the radiation energy deposition in the proximity of incident spot is always stronger. At t=20ps, radiation deposition was confined in a narrow region around the laser spot. At t=40ps, the radiative heat flux penetrated to a longer distance radially due to radiation propagation. The magnitude of divergence fields at t=20ps and at t=40ps are greater than those at t=100ps and at t=400ps, because when the incident pulse is turned off after duration time (40ps), the source of radiation only comes from the scattered radiation. As time elapses, the scattering is becoming weaker and weaker. Furthermore, at t=400ps, the order of magnitude of the divergence field in the tissue is close to 1e-31. Thus it is reasonable to assume a stable local temperature rise is achieved within t=400ps, which equals $40t_p$.

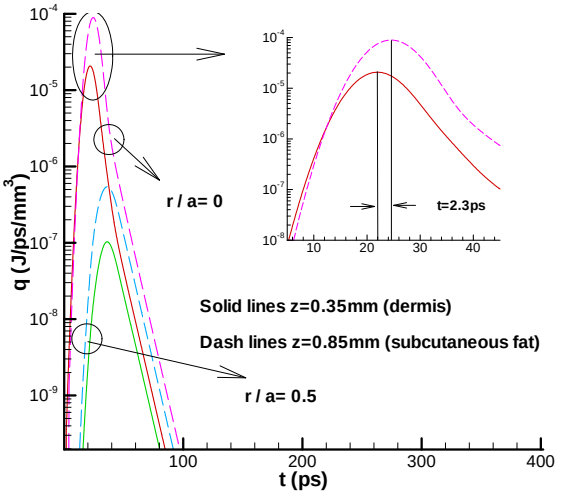

Figure 3 Temporal profiles of the divergence of radiative heat flux in dermis and subcutaneous fat layers.

Figure 3 compares the temporal profiles of the divergence of radiative heat flux in two layers of the skin tissue at different radial locations. At any location, the absorbed radiation energy increases rapidly to its maximum value with the input of short pulse laser before turn-off of the pulse ($4t_p$) and then decrease exponentially. The divergence of heat flux represents the absorbed or deposited volumetric laser energy in the medium. Since the absorption coefficient of subcutaneous fat is much greater than that of dermis, the divergence of heat flux is greater in fat layer, although it is behind the dermis layer.

Since the refractive index is assume to be 1.4 for all skin layers[16], the speed of light in the tissue is approximately evaluated as 0.214mm/ps. In the small figure, the time lag between two peaks represents the flight time of the laser in a certain part of the tissue. So it took 2.3ps for the pulse laser to pass through a distance as Δz=0.85-0.35=0.5mm.

The local temperature response depends on the local volume average accumulation of radiation energy absorption. As we can see from Fig.4, the region with a higher absorption coefficient (e.g. z=0.35mm) or closer to laser incident spot (e.g. r/a=0) will have higher temperature increase.

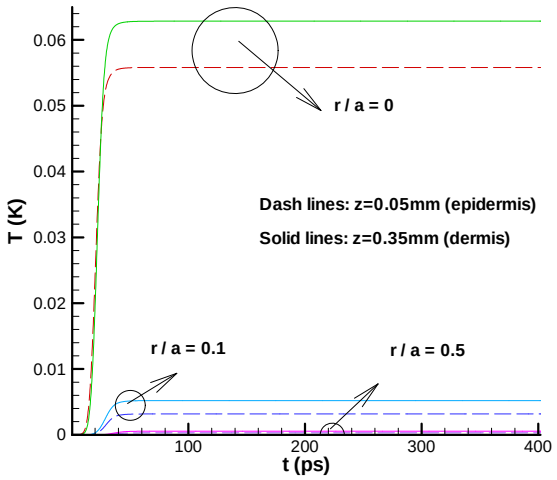

Figure 4 Temporal profiles of temperature rise in the epidermis and dermis layers subjected to an ultrafast pulse irradiation.

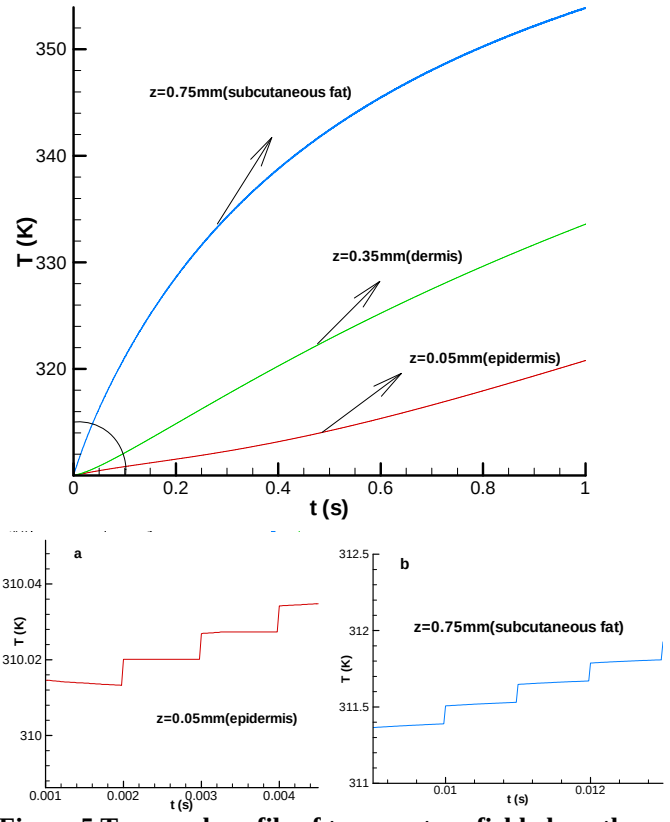

Figure 5 Temporal profile of temperature field along the cylinder centerline in three layers subjected to a pulse train with repletion rate 1 kHz: (a) epidermis; (b) subcutaneous fat.

Now let us consider transient radiative and conductive heat transfer in the non-homogeneous skin tissue subject to a pulse train. Fig.5 shows the temporal profile at three different axial locations (z=0.05, 0.35 and 0.75mm) along the centerline. Unlike the single pulse source, oscillations are observed at each temporal temperature profile. These oscillations are due to the pulse train incident on the skin tissue. A certain location in the layer of epidermis gives a rapid local temperature response to each single pulse irradiation. Then, after laser turned off, the temperature dropping is caused by the heat loss to ambient. Temperature rises again when a new pulse is incident. The strongest oscillations were found at the layer (e.g. z=0.75mm) with the highest value of absorption coefficient.

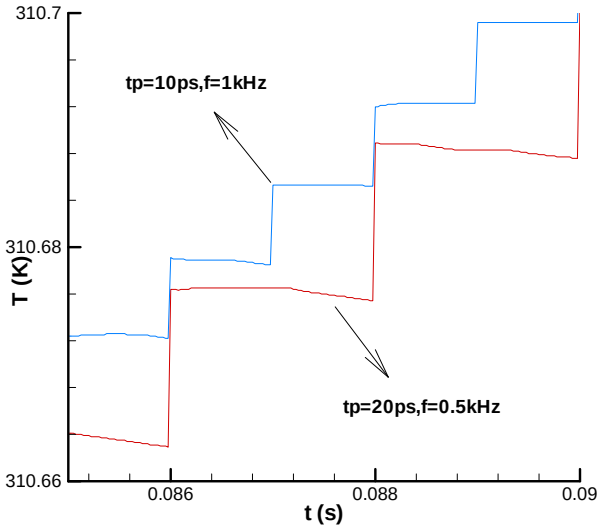

Figure 6 Temporal profiles of temperature at location r=0mm, z=0mm with different pulse widths and repetition rates.

We considered pulse duration irradiation within $4t_p$ and impinging area within $2v$. Then, the averaged incident laser power density is obtained by integrating equation (5):

$$P = \frac{N}{t_r}\frac{1}{(2v)^2}\int_0^{2v} 2r\int_0^{4t_p}\frac{I_c(r,z=0,t)}{1-R}dtdr = 0.2612\frac{I_0 N t_p}{t_r} \qquad (12)$$

where N, t_r are the number of pulses and time duration of the whole irradiation respectively; Then f=N/t_r is the repetition rate of the pulsed laser.

The effect of pulse train repetition rate is studied by varying the pulse train frequency f (0.5, 1 kHz). According to equation (12), the total averaged incident laser power density is kept constant for the two cases. A lower frequency (e.g. 0.5 kHz) means a greater amount of energy was injected into the skin tissue during a longer time lag between two successive pulses irradiating. In Fig.6, a stronger temperature fluctuation is found for the case f=0.5 kHz. Furthermore, larger amount of heat loss is caused by the longer time for skin tissue exchanging the heat energy with the ambient through the incident surface. Since the total energy is the same for both cases, the temporal temperature at the origin point of the tissue cylinder is lower for the skin tissue subject to a lower repetition rate (e.g. 0.5 kHz) than that of the tissue subject to a higher repetition rate (e.g. 1 kHz).

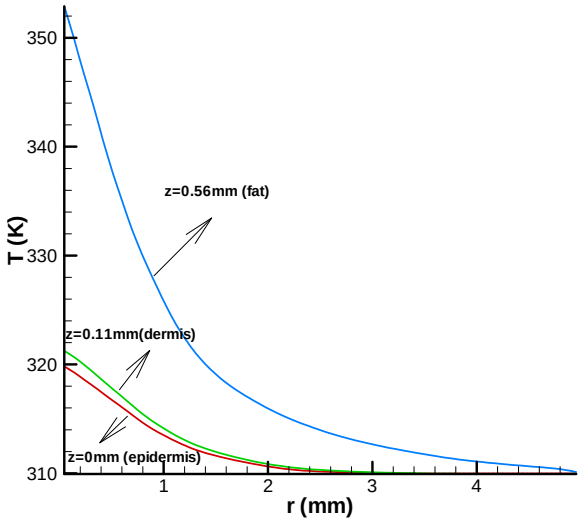

Figure 7 Temperature profile along the radial direction at different axial locations at 1s when the tissue subjected to the pulse train with repetition rate 1 kHz.

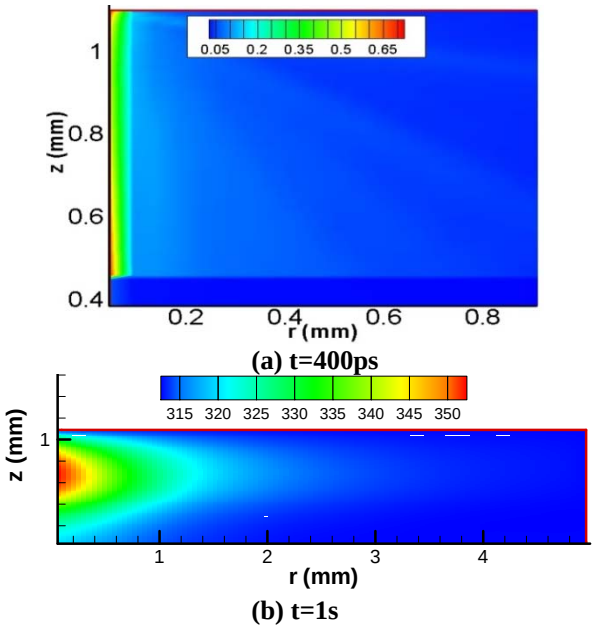

Figure 8 Contours of temperature rise at t=400ps (a) (top left corner of the tissue cylinder); temperature field in the skin tissue subject to pulse train (1 kHz) at t= 1s (b).

Figure 7 shows the temperature distribution along three layer's surface at the time instant t=1s. The temperature along the incident surface (z=0mm) is the lowest comparing with these two layers. The temperature along each surface reaches its

peak at the centerline and decreases to its minimum value due to the heat transfer with ambient. At the end, all three curves converge to constant temperature 310K at r=a because of the constant temperature boundary there.

Figure 8 also gives a clear view about the instant temperature distribution in the skin tissue. Before t=400ps, the local temperature rise totally depends on irradiation deposition. So the maximum temperature increase is confined to superficial regime along the centerline in the fat layer, Fig.8 (a). After that, due to multiple pulse irradiations and thermal diffusion, the thermal energy propagates both radially and axially in the skin tissue, Fig 8 (b).

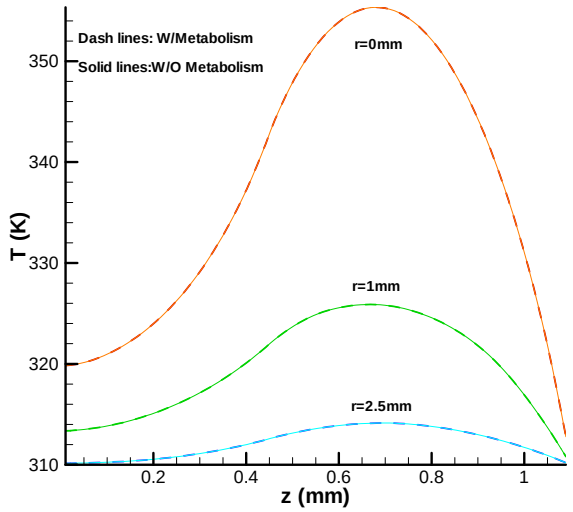

Figure 9 Temperature profile along the axial location at different radial location at 1s when the tissue is subjected to the pulse train with repetition rate 1 kHz.

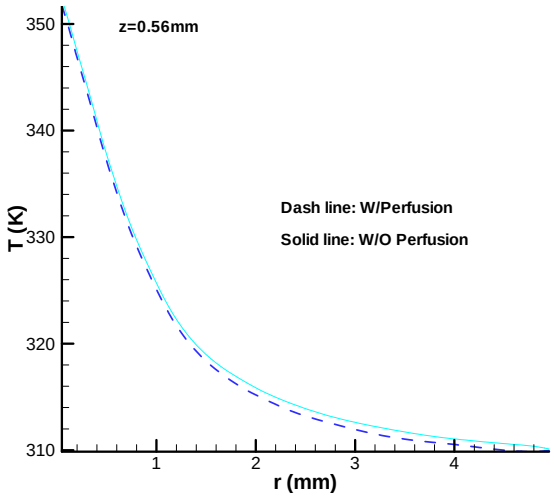

Figure 10 Temperature profile along the radial direction at z=0.56mm at 1s when the tissue subjected to the pulse train with repetition rate 1 kHz.

The effects of blood perfusion rate and metabolic heat generation are also discussed in this study. In Figs. 9 and 10, very tiny differences are found between skin tissues with and without metabolic heat generation or blood perfusion rate. This is because in the skin tissue not only metabolic generation but also blood perfusions are not effective comparing with the strong incident laser intensity. Unlike the metabolic generation's single role as a heat source all over the tissue cylinder, blood perfusion rate plays as a heat sink as we can see from Fig. 10. Because supplying arterial blood temperature is specified as 310K, so in the region where temperature is greater than 310k, the blood perfusion can be treated as a cooler.

5. CONCLUSION

A combined time-dependent radiation and Pennes's conduction model is developed and employed to predict the temperature field in the multi-layer skin tissue subject to a train of short pulse radiation. The model integrates two steps. In the first step, the radiative transfer process of a multi-layer skin tissue subject to a single short pulse is simulated. Pseudo steady temperature respond in the tissue is found within 400ps. In the second step, thermal diffusion is considered between two successive short pulse irradiations at the meso-time scale. The procedure is repeated for each pulse of the pulse train. The conduction calculation is continuous during the whole heat transfer process while the radiation heat transport in the tissue irradiate by each pulse is calculated just for one time. Then the local temperature respond caused by radiation energy accumulation there can be added as a temperature rise with the onset of a new pulse incident on the skin tissue.

The radiative energy distribution pattern in the tissue induced by a single pulse irradiation depends strongly on the absorption coefficient and scattering coefficient. As for the three different layers considered in this model, the subcutaneous fat has the largest absorption coefficient which is almost one order of magnitude higher than the other two layers'. Thus, most of the radiative energy is accumulated in the fat layer. As time elapses, scattered radiation penetrates to the deep tissue.

The characteristics of the skin tissue subject to a pulse train irradiation are also investigated. The temporal temperature profile goes up and down repetitively due to the pulse incident and the heat losses to ambient and surrounding tissue. Strong temperature fluctuation with a lower maximum temperature value is observed when the tissue is irradiated by a pulse train with lower repetition rate and vice versa.

Pennes' bio-heat transfer model is adopted to predict the temperature field of the skin tissue between two successive pulse irradiations. Blood perfusion rate and metabolic generation play different roles in the perfused tissue. As for the skin tissue, comparing with the strong incident intensity of pulse laser, both the blood perfusion rate and metabolic generation are found to be negligible.

REFERENCES

1. R.R. Anderson, J.A. Parrish, *Selective photothermolysis: precise microsurgery by selective absorption of pulsed radiation.* Science, 1983. **220**: pp. 524-527.
2. M.H. Niemz, *Laser-Tissue Interactions*. 1996, Springer: New York.
3. L.S. Bass, M.R. Treat, *Laser tissue welding: a comprehensive review of current and future applications.* Lasers Surg. Med, 1995. **17**: pp. 315–349.
4. R.R. Anderson, *Dermatological history of the ruby laser: thelong story of short pulses.* Arch. Dermatol, 2003. **139**: pp. 70-74.
5. Y. Yamada, *Light-tissue interactions and optical imaging in biomedicine.* Annu. Rev. Heat Transfer 1995. **6**: pp. 1-59.
6. H. Quan, Z. Guo, *Fast 3-D optical imaging with transient fluorescence signals.* Opt. Express 2004. **12**: pp. 449-457.
7. Z. Guo, S.K. Wan, D.A. August, J. Ying S.M. Dunn, J.L.Semmlow, *Optical imaging of breast tumor through temporal log-slope difference mappings.* Comput. Biol. Med., 2006. **36**: pp. 209-223.
8. S. Kumar, K. Mitra, *Microscale aspects of thermal radiatin transport and laser applications.* Adv. Heat Transfer, 1999. **33**: pp. 187-294.
9. Z. Guo, S. Kumar, *Radiation element method for transient hyperbolic radiative transfer in plane-parallel inhomogeneous media.* Numer. Heat Transfer, 2001. **Part B 39**: pp. 371-387.
10. Z. Guo, S. Kumar, K.C. San, *Multi-dimensional Monte Carlo simulation of short pulse laser radiatin transport in scattering media.* J. Thermophys. Heat Transfer, 2000. **14**: pp. 504-511.
11. Z. Guo, S. Kumar, *Discrete-ordinates solution of short-pulsed laser transport in two-dimensional turbid media.* Appl. Opt, 2001. **40**: pp. 3156-3163.
12. Z. Guo, S. Kumar, *Three-dimensional discrete ordinates method in transient radiative transfer.* J. Thermophys. Heat Transfer, 2002. **16**: pp. 289-296.
13. K. Kim, Z. Guo, *Multi-time-scale heat transfer modeling of turbid tissues exposed to short-pulsed irradiations.* Computer Methods and Programs in Biomedicine, 2007. **86**: pp. 112-123.
14. H. Arkin, L.X. Xu, K.R. Holmes, *Recent developments in modeling heat transfer in blood perfused tissues.* IEEE Trans. Biomed. Eng., 1994. **41**: pp. 97-107.
15. A. F. Emery, K.M.Sekins, *The use of heat transfer principles in designing optimal diathermy and cancer treatment modalities.* Int. Journal of Heat and Mass Transfer, 1982. **25**(6): pp. 823-834.
16. E. Salomatina, B. Jiang, J. Novak, A.N.Yaroslavsky, *Optical properties of normal and cancerous human skin in the visible and near infrared spectral range.* Journal of Biomedical Optics, 2006. **11**(6): pp. 261-269.
17. M.L. Cohen, *Measurement of the thermal properties of human skin.* Journal of investigative dermatology, 1977. **69**(3): pp. 333-337.
18. K.H. Kim, Z. Guo, *Ultrafast radiation heat transfer in laser tissue welding and soldering.* Numer. Heat Transfer, 2004. **Part A 46**: pp. 23-46.
19. D.A. Anderson, J.C. Tannehill, R.H. Pletcher, *Computational Fluid Mechanics and Heat Transfer*, in *computational methods in mechanics and thermal science*. 1984, Hemisphere Publishing Corporation: Washington.